Cellulose Nanocrystals Obtained From Microcrystalline Cellulose by p-toluene Sulfonic Acid Hydrolysis, NaOH and Ethylenediamine Treatment

Songlin Wang (wangsongl@126.com)
Qingdao University of Science and Technology
Qian Wang
Qingdao University of Science and Technology
Yao Kai
Qingdao University of Science and Technology

Research Article

Keywords: Cellulose nanocrystals, Allomorph, P-toluene sulfonic acid, Thermal stability, Crystallinity index, Zeta potential

Posted Date: September 22nd, 2021

DOI: https://doi.org/10.21203/rs.3.rs-918157/v1

Version of Record: A version of this preprint was published at Cellulose on January 7th, 2022. See the published version at https://doi.org/10.1007/s10570-021-04409-1.

Abstract

Cellulose nanocrystals (CNC) were first isolated from microcrystalline cellulose (MCC) by p-toluene sulfonic acid (p-TsOH) hydrolysis. Cellulose II nanocrystal (CNC II) and cellulose III nanocrystal (CNC III) were then formed by swelling the obtained cellulose I nanocrystal (CNC I) in concentrated sodium hydroxide solutions and ethylenediamine (EDA) respectively. The properties of CNC I, CNC II and CNC III were subjected to comprehensive characterization by Fourier-transform infrared spectroscopy (FTIR), X-ray diffraction (XRD), scanning electron microscope (SEM), transmission electron microscopy (TEM), and thermogravimetric analysis (TGA). The results indicated that CNC I, CNC II and CNC III obtained in this research had high crystallinity index and good thermal stability. The degradation temperatures of the resulted CNC I, CNC II and CNC III were 300 ℃, 275 ℃ and 242 ℃, respectively. No ester bonds were found in the resulted CNC. CNC prepared in this research also had large aspect ratio and high negative zeta potential.

1. Introduction

Cellulose, the most abundant and renewable natural polymer resource in the world, is widely used nowadays for the production of daily used products and materials. Due to its low cost, availability, renewability, and unique morphology, it attracts more and more research efforts in recent years (Brinchi et al., 2013; Shao, Wang, Chang, Xu & Yang, 2017; Zander, Dong, Steele & Grant, 2014). Further reducing the cellulose size to nanometer range, it exhibits excellent properties such as low density, high modulus, high strength and high hydrophilicity due to the intra- and inter-molecular hydrogen bonds formed by the large number of hydroxyl groups on celluloses making the cellulose molecular chains tightly bound together (Lee et al., 2009; Mariño, Lucimara, Durán & Tasic, 2015). However, cellulose has certain defects, for example, poor performance under certain chemical conditions, low mechanical strength and low dimensional stability. Therefore, cellulose I nanocrystal (CNC I) is widely used in gel (Aulin, Netrval, WåGberg & Lindströmc, 2010; Huang et al., 2018), photoelectric (Lv et al., 2019; Miettunen et al.,2014), energy storage (Zhu et al., 2016), medicine (Carlsson et al., 2012; Dieter et al., 2010), functional materials (Mishra et al., 2018) and other areas. Both suballomorphs of CNC I, namely I_α and I_β can be converted to cellulose II nanocrystal (CNC II) and cellulose III nanocrystal (CNC III) through thermochemical processing. CNC II can be formed by well established mercerization process, which consists of swelling CNC I in concentrated sodium hydroxide solutions for certain amount of time followed by removing the swelling agent. It is not only an important method for producing viscose fiber and carboxymethyl cellulose, but has its significance for cellulose activation. Compared to the parallel up arrangement of CNC I, the antiparallel chains arrangement in CNC II result in a more stable and preferable structure for various textiles and paper application. Due to its lower crystallinity index, CNC III usually demonstrates a higher reactivity than CNC I and CNC II for the preparation of cellulose derivatives (Habibi & Vignon, 2008). Because of the different crystal form of CNC, CNC derivatives with different properties can be obtained. Converting CNCs from cellulose I to cellulose II and cellulose III, its crystallinity index and the

crystallite size decreased and the internal surface area increased while Young's modulus of the fiber decreased and the ultimate strain increased (Ishikawa, Okano & Sugiyama, 1997).

At present, mechanical methods (Faradilla et al., 2017; Lichtenstein & Lavoine, 2017) and chemical methods are commonly used to prepare CNC. The native nanocellulose prepared by mechanical approach which requires high energy consumption has crystalline and amorphous regions with a wide size distribution. In order to reduce the production cost, chemical or enzymatic pretreatment were usually employed (Kelly, Herman, Maria, Mirabel & Valdeir, 2018). Acid hydrolysis and TEMPO oxidation are commonly used chemical approach (Bibin et al., 2013; Chen et al., 2017; Vasconcelos et al., 2017). Sulfuric acid (Morais et al., 2013; Roman & Winter, 2004; Poggi, Giorgi, Toccafondi, Katzur & Baglioni, 2010), phosphoric acid (Agnieszka, Radzik, Haraźna & Pielichowski, 2018) and dicarboxylic acid (Bian et al., 2017) are used for acid hydrolysis. Acid preferentially acts on the non-crystalline area while the crystalline area maintains its integrity. However, the reaction between surface hydroxyl group of crystalline area and acid radical groups during sulfuric acid hydrolysis process reduced thermal stability. Some researches were conduct to modify resulted CNC I from sulfuric acid hydrolysis in order to improve the thermal stability of CNC (Wu, Xu, Gong, Li & Mo, 2018).

Our previous research has shown CNC I produced by P-toluene sulfonic acid (p-TsOH) hydrolysis of microcrystalline cellulose (MCC) with good thermal stability and high crystallinity index. CNC II and CNC III can be produced by subjecting CNC I to sodium hydroxide and ethylenediamine (EDA) treatment, respectively. To our knowledge, properties of CNC I, CNC II and CNC III produced by such approaches have not been reported. In this work, we prepared CNC allomorphs and these samples were analyzed in terms of crystallinity index, particle size, zeta potential, morphology and thermal stability, etc.

2. Experimental

2.1 Materials

Microcrystalline cellulose (MCC) (particle size about 50 μm, Chengdu Kelong Chemically pure Chemical Co., Ltd., Chengdu, China) was used as raw material for producing cellulose nanocrystals (CNCs). p-TsOH (analytically pure) was purchased from Tianjin Bodie Chemical Co., Ltd., Tianjin, China. Analytically pure NaOH was purchased from Tianjin Beichen Fangzheng Reagent Factory, Tianjin, China. Analytically pure ethylenediamine (EDA) was purchased from Tianjin Yongda Chemical Reagent Co., Ltd., Tianjin, China. All the chemicals were used directly without further purification.

2.2 CNC I obtained by p-toluene sulfonic acid (p-TsOH) hydrolysis of microcrystalline cellulose (MCC)

5.0 g MCC was added to 75 mL p-TsOH solution. The reaction was allowed to proceed at 70°C for 4 h according to the pre-designed experimental conditions. At the end of reaction, 100 mL of distilled and deionized water was added to quench the reaction. The sample obtained by acid hydrolysis was then washed with deionized water using repeated centrifuge cycles (10 min at 4,000 rpm). The last wash was conducted using dialysis with deionized water until the wash water reaching constant pH. The obtained

CNCs suspension was lyophilized for three days to obtain solid CNCs. The spent acid was recovered by crystallization.

2.3 CNC II prepared by NaOH treatment

1.0 g above-mentioned CNC I was placed in 50 mL 18.5 wt% NaOH solution under continuous stirring at 300 rpm for 1.5 h. The sample was dialyzed with distilled water until the pH was constant. The obtained white precipitate was freeze-dried to obtain CNC II.

2.4 CNC III prepared by EDA treatment

1.0 g above-mentioned CNC I was placed in 50 mL room temperature EDA solution for 24h with continuous stirring at 300 rpm. The sample was dialyzed against methanol until the pH was constant. The obtained white precipitate was freeze-dried to obtain CNC III.

2.5 Particle size and zeta potential of CNC allomorphs

To compare the particle size and surface charge of CNC allomorphs, the size and zeta potential of the CNC was measured using particle size analyzer (Malvern Zetasizer Nano series, Malvern, UK). All suspensions were dispersed to a concentration of 0.2 wt% at room temperature before analysis.

2.6 Scanning electron microscopy (SEM) and transmission electron microscopy (TEM) analysis of CNC allomorphs

The SEM images of CNC allomorphs were recorded by a field-emission scanning electron microscope (SEM) (JSM-6380, Jeol, Akishima, Tokyo, Japan). A droplet of 0.01% w/v sonicated CNC dispersion was placed on a conductive aluminum plate. Then the excess water was removed by absorbent paper and subsequently dried in air. The sample was sputter coated with gold (Hitachi E-1010 Ion Sputtering System, Tokyo, Japan) for 120 s to provide sufficient conductivity under vacuum.

The TEM image of CNC allomorphs were recorded at room temperature by transmission electron microscope (JEM-2100PLUS, Japan JEOL Company, Akishima, Tokyo, Japan) under an acceleration voltage of 200 kV. 10 µL suspension was deposited on a discharged carbon-coated grid and the excess liquid was removed by absorbent paper. The sample was then stained with 2% phosphotungstic acid solution. The excess dye solution was removed by absorbent paper and the dried at room temperature for observation.

2.7 X-ray diffraction (XRD) analysis and crystallinity index calculation

The XRD patterns for all CNC allomorphs were obtained with an X-ray diffractometer ((Rigaku D/Max 2500 v/PC system, Rigaku Corporation, Tokyo, Japan) using a Cu Kα radiation at 40 kV and 30 mA (I = 0.154 nm). Scattered radiation was detected in the range of $2\theta = 5^{o} - 40^{o}$ at a scan rate of 4^{o}/min. XRD data were analyzed using software MDI Jade 6.0. Area integration method was used to calculate the

crystallinity index of the CNC (Song et al.,2016). The crystallinity index was calculated as the ratio of the area of the cellulose crystal region to the total area of the XRD pattern.

2.8 Fourier Transform Infrared Spectroscopy (FTIR) analysis

The FTIR spectra of the sample was collected by Fourier transform infrared spectrometer (VECTOR22, Germany Bruker Co., Ettlingen, Germany) using a KBr disc containing finely ground samples (1%). The resolution of infrared spectrum is 4 cm^{-1}, the collection range is 500-4000 cm^{-1} and the spectra is obtained from 8 scans in transmission mode.

2.9 Thermogravimetric analysis (TGA)

Thermogravimetric analysis (TGA) was performed using a thermogravimetric analyzer (TAQ-500, Shimadzu Co., Kyoto, Japan). All samples were heated from 25°C to 800°C at a rate of 10°C/min under a nitrogen atmosphere (30 mL/min).

3. Results And Discussion

3.1 Yield and Zeta potential of CNC I

As seen from Fig. 2, the yield and Zeta potential of CNC I increased with the increase of p-TsOH mass concentration and temperature. Less stable suspension was obtained with the increase of acid concentration as the absolute value of the zeta potential getting smaller. A dark and yellow product was obtained as the temperature and p-TsOH mass concentration increased. Therefore, the reaction temperature and acid concentration should be controlled to prevent the cellulose from being over hydrolyzed. Fig. 3 shows the potential distribution diagram.

3.2 CNC I particle size analysis

The particle size of CNC I can be seen from Fig. 4. As the p-TsOH mass concentration and reaction temperature increased, the particle size of CNC I gradually decreased. This is probably because of the higher degree of hydrolysis at higher reaction temperature and acid concentration.

Table 1

Fiber width and length, and the aspect ratio of CNC allomorphs

Sample	Width (nm)	Length (nm)	length to diameter ratio
CNC I	9.1	368.9	40.5
CNC □	21.8	330.4	15.2
CNC □	27.8	321.3	11.6

The width, diameter and aspect ratio of CNC are shown in Table 1. The aspect ratios of CNC I, CNC II and CNC III were 40.5, 15.2, and 11.6, respectively. The larger the aspect ratio, the better the mechanical reinforcement effect. Thus, CNC I can provide better mechanical reinforcement effect compared to CNC II and CNC III.

3.3 SEM and TEM analysis of CNC allomorphs

Fig. 5 shows the different morphologies of CNC allomorphs. As seen from the Figure, CNC is rod-shaped and interwoven into a network structure. These characteristics can be used as a reinforcing agent in composite materials. The length of CNC I was about 100 - 200 nm and the width was 40 - 80 nm. CNC II had a shorter and wider morphology than CNC I, and the size of CNC III was in the middle of these two. Self-assembly and self-aggregation occurred in the process of freeze drying thus increased the CNC size. The surface of the alkali-treated CNC was smoother, while the surface corrosion induced by alkali and organic amine molecules followed, and the van der Waals bond between them also be broken during the crystal form transformation, which led to some kinks as shown by the SEM image of CNC □ and CNC □.

Fig. 6 shows the TEM images of the CNC allomorphs. The CNC I with a typical short rod-like shape were entangled. Although crystal form changed after sodium hydroxide and EDA treatment, CNC of different crystal forms still maintained rod-like shape and the average width was not much different from that of CNC I. This is probably because only a single cellulose microfibril underwent crystal form change and did not affect the adjacent microfibrils after alkali and EDA treatment. CNC II and CNC III had same molecular chain arrangement as CNC I.

3.4 Integral crystallinity index analysis of CNC allomorph

The crystallinity index of CNC allomorphs was analyzed by XRD. As shown in Fig. 7, X-ray diffraction patterns of CNC allomorph reflect the crystal integrity of each crystal form. The diffraction peak positions of CNC I were at 15.0°, 16.4°, and 22.5°, corresponding to (110), ($1\bar{1}$ 0), and (200) crystal planes, respectively. The diffraction peak positions of CNC II were at 12.0°, 20.0°, and 21.6°, corresponding to ($\bar{1}$ 10), (110), and (020) crystal planes, respectively, indicating the successful conversion of CNC I to CNC II. Faint peaks of CNC I (15.0°, 16.4°, 22.5°) were detected in the XRD diffraction spectrum of CNC III. However, the main peaks of 12.0°,17.2° and 21.0° corresponds to (010), (002) crystal planes and (100). (012), ($1\bar{1}$ 0) composite crystal planes of CNC III are more obvious. Therefore, it can be concluded that the crystal form conversion from CNC I to CNC III has also been successfully achieved. Meanwhile, crystallinity index of these three CNC crystal forms were 89.70%, 79.55% and 58.70%, respectively. The

decrease of crystallinity index of CNC II and CNC III indicates some crystalline area was destroyed during NaOH or EDA treatment.

3.5 FTIR analysis of CNC allomorph

The infrared spectra of CNC is shown in Fig. 8. As seen from the spectra, no new functional groups were found which means that the hydrolysis of p-TsOH did not introduce new functional groups and the structure of cellulose nanocrystal was not changed. The absorption peaks of CNCs crystal form mainly appear in the range from 3700 cm^{-1} to 2600 cm^{-1} and from 1700 cm^{-1} to 800 cm^{-1}. In CNC I, the peak at 3444 cm^{-1} was caused by the stretching vibration of the free -OH group in the cellulose molecule. Absorption peaks of 2901 cm^{-1} and 1430 cm^{-1} were caused by the stretching and bending of -CHbelonging to $-CH_2$ group. Absorption peak of 1637 cm^{-1} was produced by the vibration of the -OH group in the cellulose. The weaker 896 cm^{-1} peak proved the break of β-glycosidic bond during the hydrolysis process, resulting in shorter cellulose chain and smaller size. The absorption peak of 2901 cm^{-1} belonging to -CH stretching vibration in CNC I was changed to 2982 cm^{-1} in CNC II. The absorption peak of 1429 cm^{-1} caused by the bending of -CHbelonging to $-CH_2$ group was not significant in CNC II, indicating the change of hydrogen bond and cellulose chains arrangement and stacking because of the alkali treatment. In CNC III, the -CH characteristic peak at 2900 cm^{-1} did not change, but the absorption peak at 1637 cm^{-1} was weakened, indicating that the EDA treatment had changed the crystal form of CNC I and reduced the amount of -OH group. The absorption peak of 1429 cm^{-1} caused by the bending of -CH belonging to $-CH_2$ group was not significant in CNC Ⅲ. These changes indicated EDA treatment changed the hydrogen bond and cellulose chains arrangement. Compared to the peak intensities at 1637 cm^{-1} and 3444 cm^{-1} of the three different crystal forms, CNC III had the highest intensity indicating CNC III had better reactivity, while the peak intensity of CNC II decreased implying its highest stability among these three crystal forms.

3.6 Thermogravimetric analysis of CNC allomorph

Fig. 9 shows the CNC thermogravimetric curves of CNC allomorph. CNC obtained by p-toluene sulfonic acid (p-TsOH) hydrolysis of microcrystalline cellulose and concentrated NaOH and ethylenediamine (EDA) treatment showed improved thermal stability. CNC I prepared by traditional sulfuric acid method generally started to degrade at a temperature of 160 °C, resulting in a mass loss of about 40% then started to degrade the remaining part at 260 °C. However, no mass loss was observed for CNC I prepared by p-TsOH until 300 ℃ and the thermal weight loss generally happened between 300 ℃ and 400 ℃, which also proved that p-TsOH hydrolysis did not introduce new group to cellulose, but only existed as a catalyst.

The change from CNC I to CNC II and CNC III reduced the thermal stability of CNC to a certain extent. When CNC I was converted to CNC II and CNC III, the initial thermal degradation temperature decreased

from 300 °C to 275 °C and 242 °C, respectively. It became easier to lose water during heating as more -OH exposed after subjecting CNC I to alkali treatment.

4 Conclusion

This work reported the preparation of cellulose nanocrystals (CNC) by p-toluene sulfonic acid (p-TsOH) hydrolysis of microcrystalline cellulose and concentrated NaOH and ethylenediamine (EDA) treatment. The obtained CNC I, CNC II and CNC III showed better thermal stability compared to those obtained by traditional sulfuric acid method. No mass loss was observed for CNC I prepared by p-TsOH until 300 ℃. The thermal degradation temperature of CNC II and CNC III occurred at 275 °C and 242 °C, respectively. The resulted CNCs had a high crystallinity index, high aspect ratio and no ester bonds was observed. The zeta potential of CNCs reached -37.9 mV, indicating the potential stability of its colloidal system.

Declarations

Acknowledgments

The project is supported by the Foundation of Guangxi Key Laboratory of Clean Pulp & Papermaking and Pollution Control, College of Light Industry and Food Engineering, Guangxi University (No. 2019KF12), and the Shandong Province of China Key Research and Development Project (No. 2019GGX102026).

References

Aulin, C., Netrval, J., WåG Be Rg, L., & Lindströmc, T. (2010). Aerogels from nanofibrillated cellulose with tunable oleophobicity. Soft Matter, 6(14), 3298-3305.

A Leszczyńska, Radzik, P., Haraźna, K., & Pielichowski, K. (2018). Thermal stability of cellulose nanocrystals prepared by succinic anhydride assisted hydrolysis. Thermochimica Acta, 663145-156.

Bibin M. C., Alcides L. L., Marcia R. D. M. C., Sivoney F. D. S., Mohini S., & Suresh S. N. (2013). Environmental ageing studies of chemically modified micro and nanofibril phenol formaldehyde composites. Industrial Crops and Products, 49(4), 471-483.

Brinchi, L., Cotana, F., Fortunati, E., & Kenny, J. M. (2013). Production of nanocrystalline cellulose from lignocellulosic biomass: technology and applications. Carbohydrate polymers, 94, 154-169.

Bian, H., Chen, L., Dai, H., & Zhu, J. Y. (2017). Integrated production of lignin containing cellulose nanocrystals (LCNF) and nanofibrils (LCNF) using an easily recyclable di-carboxylic acid. Carbohydrate Polymers, 167, 167-176.

Carlsson, D. O., Nystršm, G., Ferraz, N., Nyholm, L., Mihranyan, A., StrøMme, M. (2012). [p1.028] development of nanocellulose/polypyrrole composites towards blood purification. Procedia Engineering, 44, 733-736.

Chen, L., Dou, J., Ma, Q., Li, N., Wu, R., & Bian, H., et al. (2017). Rapid and near-complete dissolution of wood lignin at ≤80℃ by a recyclable acid hydrotrope. Science Advances, 3(9), e1701735.

Dieter, Klemm, Friederike, Kramer, Sebastian, & Moritz, et al. (2010). Nanocelluloses: a new family of nature-based materials. Angewandte Chemie International Edition, 50, 5438-5466.

Faradilla, R., Lee, G., Arns, J. Y., Roberts, J., & Arcot, J. (2017). Characteristics of a free-standing film from banana pseudostem nanocellulose generated from tempo-mediated oxidation. Carbohydrate Polymers, 174, 1156-1163.

Habibi, Y., & Vignon, M. R. (2008). Optimization of cellouronic acid synthesis by tempo-mediated oxidation of cellulose from sugar beet pulp. Cellulose, 15(1), 177-185.

Huang, W., Wang, Y., Huang, Z., Wang, X., Chen, L., & Zhang, Y., et al. (2018). On-demand dissolvable self-healing hydrogel based on carboxymethyl chitosan and cellulose nanocrystal for deep partial thickness burn wound healing. ACS Applied Materials & Interfaces, 10(48), 41076-41088.

Ishikawa, A., Okano, T., & Sugiyama, J. (1997). Fine structure and tensile properties of ramie fibres in the crystalline form of cellulose I, , , II and IvI. Polymer, 38(2), 463-468.

Kelly Cristina Coelho de Carvalho Benini a, A, H. J. C. V., Maria Odila Hilário Cioffi a, B, M. C. R., & C, V. A. (2018). Preparation of nanocellulose from imperata brasiliensis grass using taguchi method - sciencedirect. Carbohydrate Polymers, 192, 337-346.

Lee, SY, Mohan, DJ, Kang, & IA, et al. (2009). Nanocellulose reinforced pva composite films: effects of acid treatment and filler loading. FIBER POLYM, 10(1), 77-82.

Lichtenstein, K., & Lavoine, N. (2017). Toward a deeper understanding of the thermal degradation mechanism of nanocellulose. Polymer Degradation & Stability, 146, 53-60.

Lv, Y., Zhou, Y., Shao, Z., Liu, Y., Wei, J., & Ye, Z. (2019). Nanocellulose-derived carbon nanosphere fibers-based nanohybrid aerogel for high-performance all-solid-state flexible supercapacitors. Journal of Materials ence Materials in Electronics, 30(9), 8585-8594.

Morais, J., Rosa, M., de Souza Filho, Men de sá Moreira, Nascimento, L. D., Nascimento, D. D., & Cassales, A. R. (2013). Extraction and characterization of nanocellulose structures from raw cotton linter. Carbohydrate Polymers, 91(1), 229-235.

Miettunen, K., Vapaavuori, J., T honen, A., Poskela, A., Lahtinen, P., & Halme, J., et al. (2014). Nanocellulose aerogel membranes for optimal electrolyte filling in dye solar cells. Nano Energy, 8, 95-

102.

Mariño, M., Lucimara, L., N Durán, & Tasic, L. (2015). Enhanced materials from nature: nanocellulose from citrus waste. Molecules, 20(4), 5908-5923.

Mishra, R. K., Sabu, A., & Tiwari, S. K. (2018). Materials chemistry and the futurist eco-friendly applications of nanocellulose: status and prospect. Journal of Saudi Chemical Society, 22(8), 949-978.

Poggi, G., Giorgi, R., To Cc Afondi, N., Katzur, V., & Baglioni, P. (2010). Hydroxide nanoparticles for deacidification and concomitant inhibition of iron-gall ink corrosion of paper. Langmuir, 26(24), 19084-19090.

Roman, M., & Winter, W. T. (2004). Effect of sulfate groups from sulfuric acid hydrolysis on the thermal degradation behavior of bacterial cellulose. Biomacromolecules, 5(5), 1671-1677.

Song, Jin, Rojas, & Orlando, et al. (2016). On the polymorphic and morphological changes of cellulose nanocrystals (CNC-I) upon mercerization and conversion to CNC-□. Carbohydrate Polymers: Scientific and Technological Aspects of Industrially Important Polysaccharides, 143, 327-335.

Shao, C., Wang, M., Chang, H., Xu, F., & Yang, J. (2017). A self-healing cellulose nanocrystal-poly(ethylene glycol) nanocomposite hydrogel via diels-alder click reaction. Acs Sustainable Chemistry & Engineering, 5(7), 6167–6174.

Vasconcelos, N. F., Feitosa, J., Da Gama, F. M. P., Morais, J. P. S., Andrade, F. K., & de Souza Filho, Men de Sá Moreira, et al. (2017). Bacterial cellulose nanocrystals produced under different hydrolysis conditions: properties and morphological features. Carbohydrate Polymers, 155, 425-431.

Wu, Z., Xu, J., Gong, J., Li, J., & Mo, L. (2018). Preparation, characterization and acetylation of cellulose nanocrystal allomorphs. Cellulose, 25(9), 4905–4918.

Zander, N. E., Dong, H., Steele, J., & Grant, J. T. (2014). Metal cation cross-linked nanocellulose hydrogels as tissue engineering substrates. Acs Appl Mater Interfaces, 6(21), 18502-18510.

Zhu, HL, Luo, Ciesielski, PN, & Fang, et al. (2016). Wood-derived materials for green electronics, biological devices, and energy applications. CHEM REV, 116(16), 9305-9374.

Figures

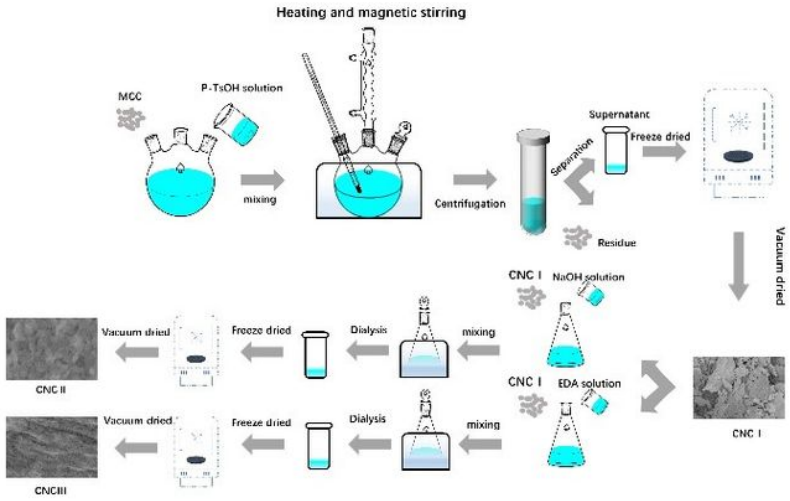

Figure 1

Schematic diagram illustrating the preparation of CNC allomorphs

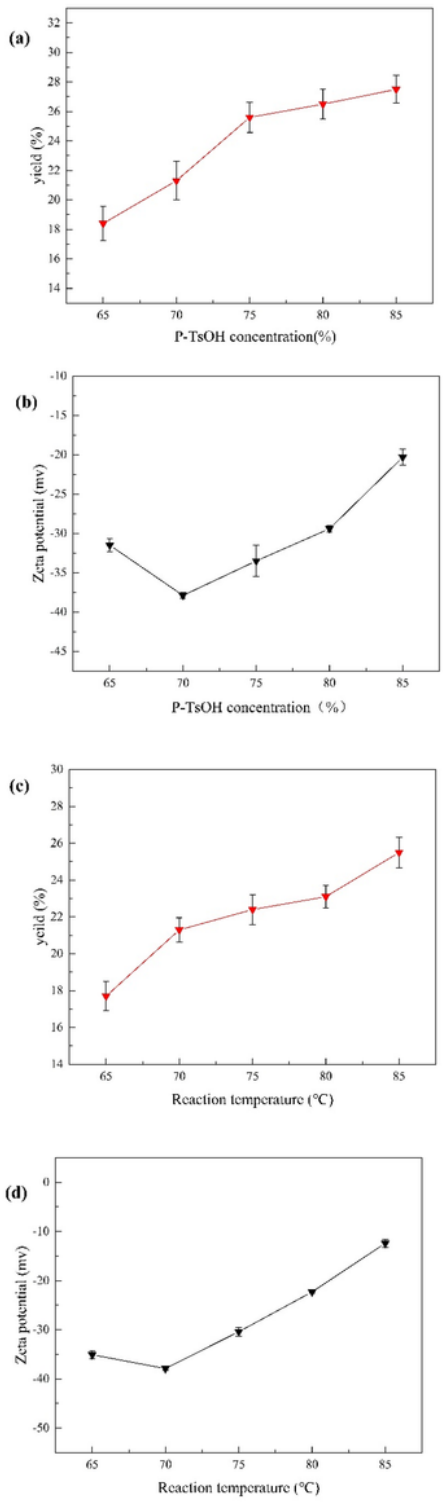

Figure 2

Yield and Zeta potential of CNC with cellulose I at different reaction conditions. (a) (b) temperature was 70; (c) (d)p-TsOH mass concentration was 70%.

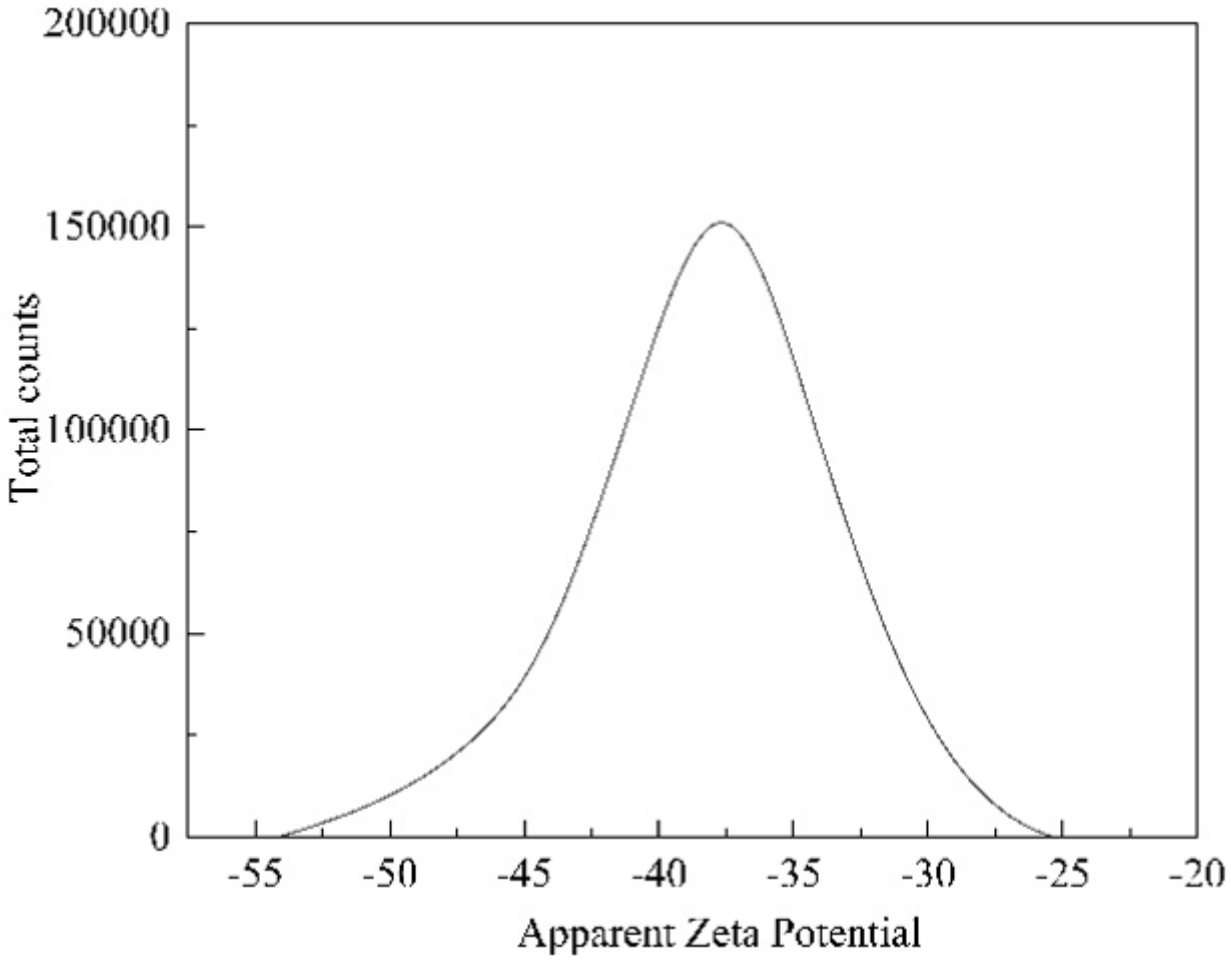

Figure 3

Potential distribution diagram (p-TsOH mass concentration was 70%, reaction temperature was 70℃ and reaction time was 1.5 h)

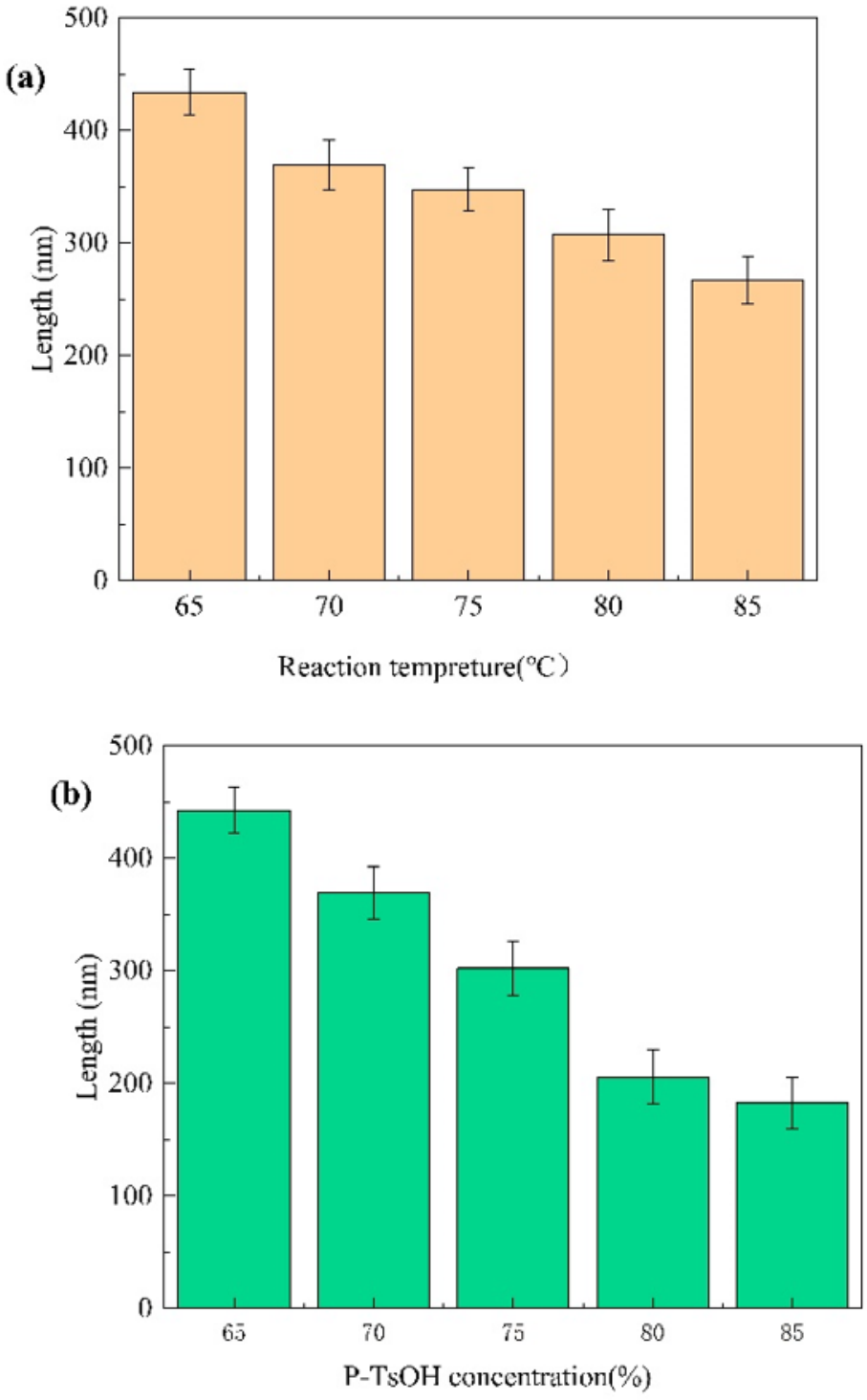

Figure 4

Particle size of CNC I. (a) p-TsOH mass concentration was 70%; (b) reaction temperature was 70°C

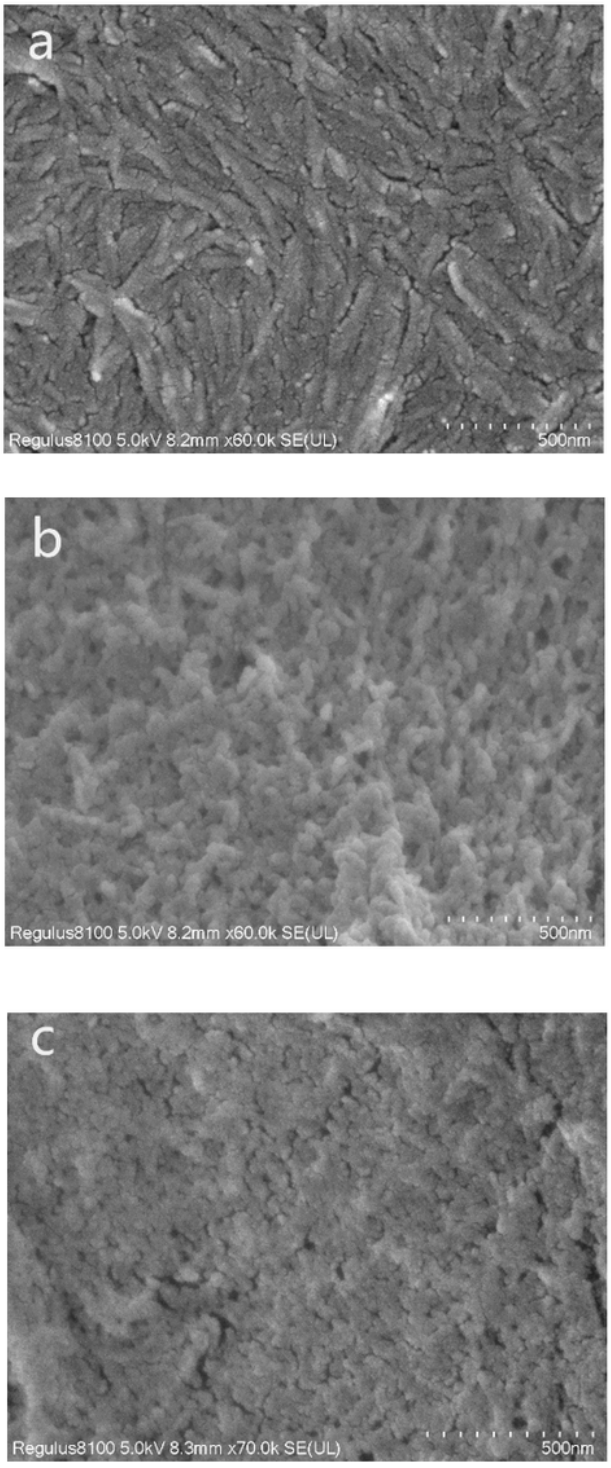

Figure 5

SEM images of samples (a) CNC I; (b) CNC II; (c) CNC III

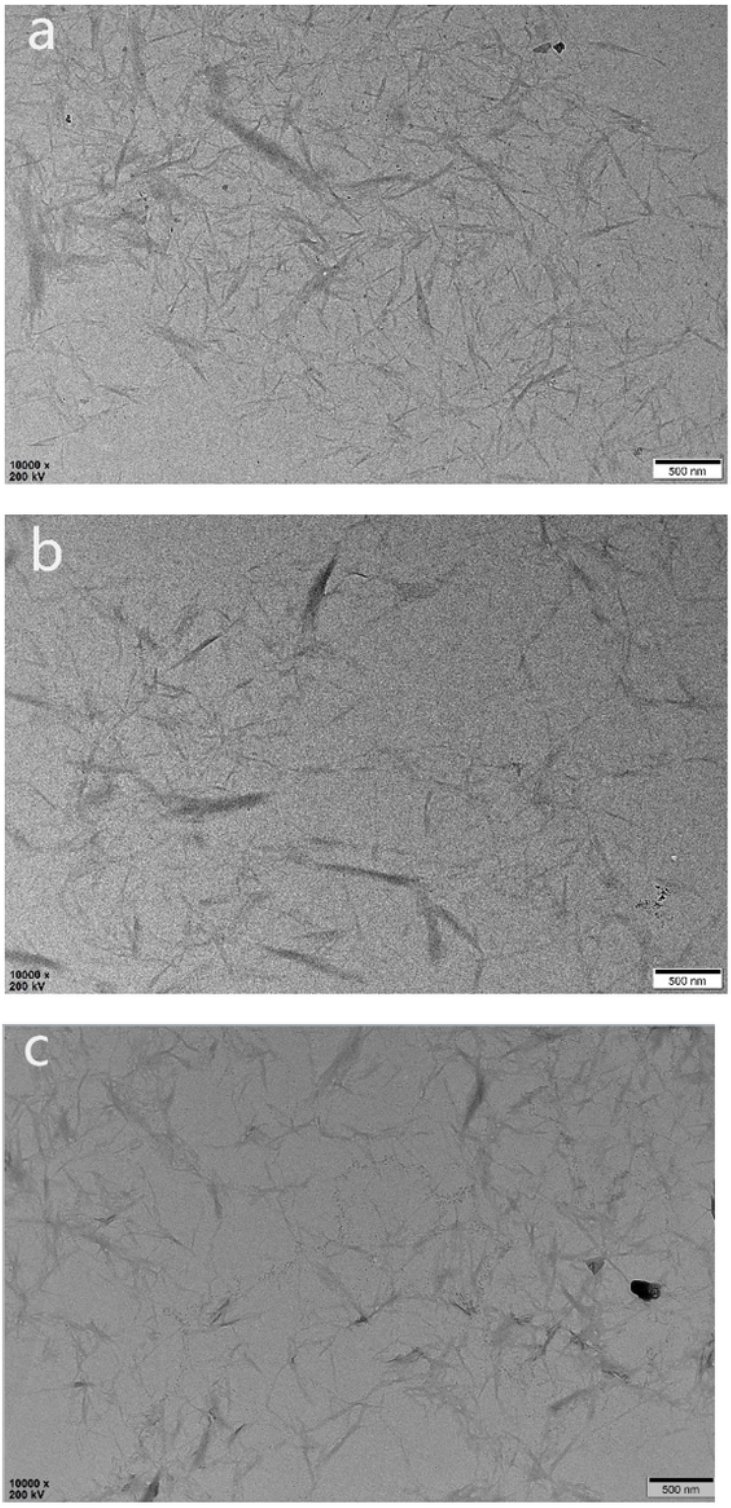

Figure 6

TEM images of samples (a).CNC I; (b). CNC II; (c).CNC III

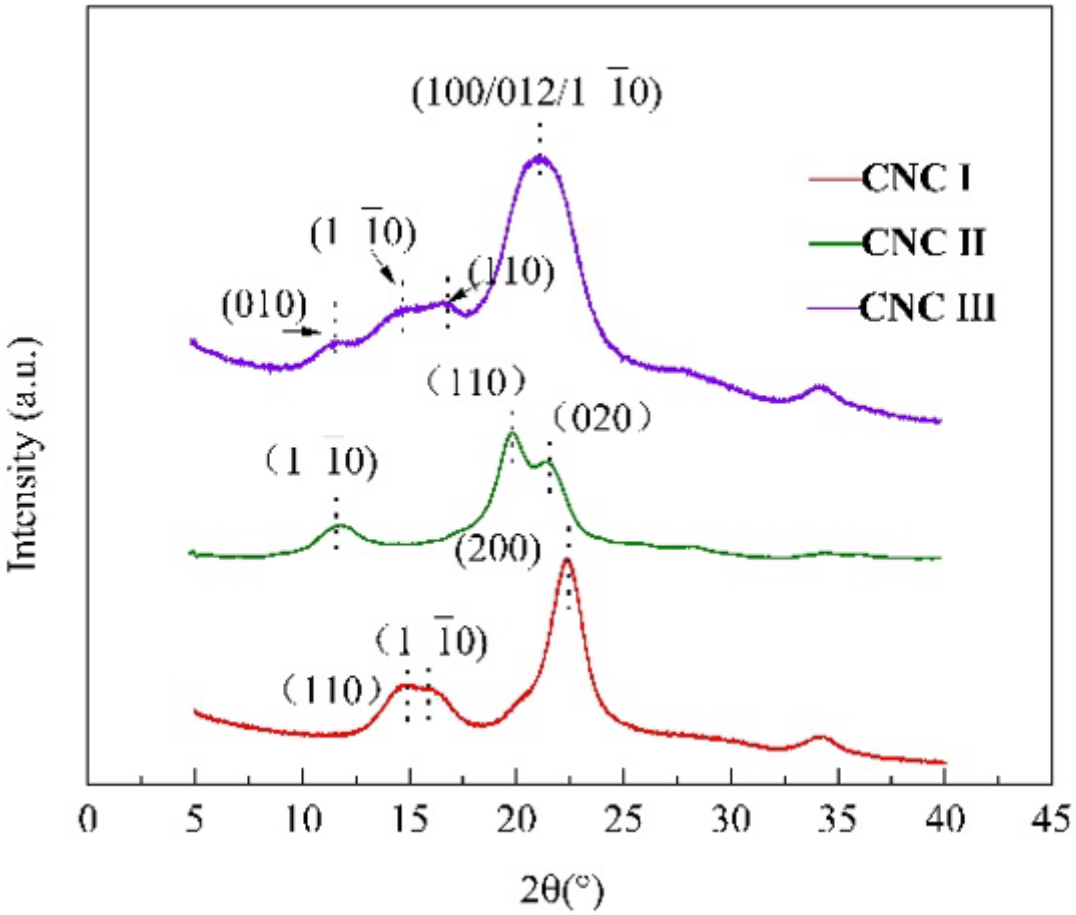

Figure 7

XRD pattens of the samples

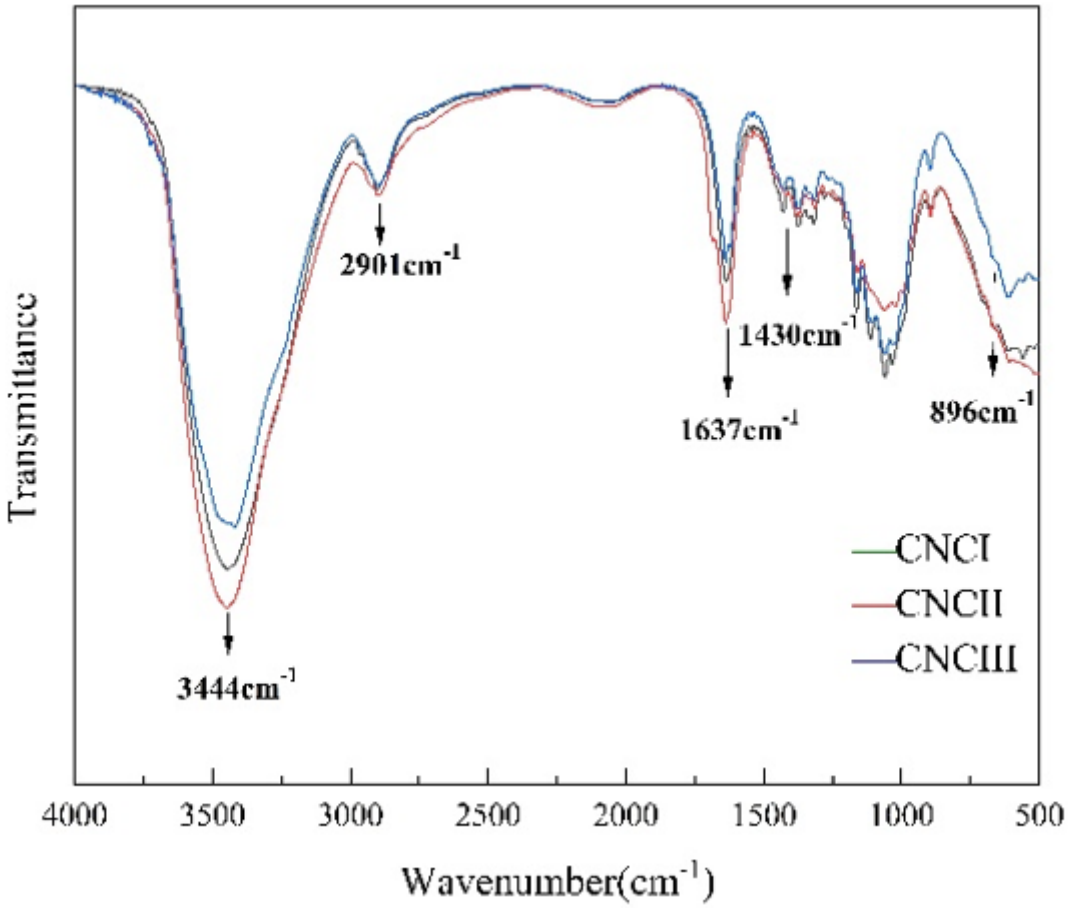

Figure 8

FTIR spectra of solid residues of the samples

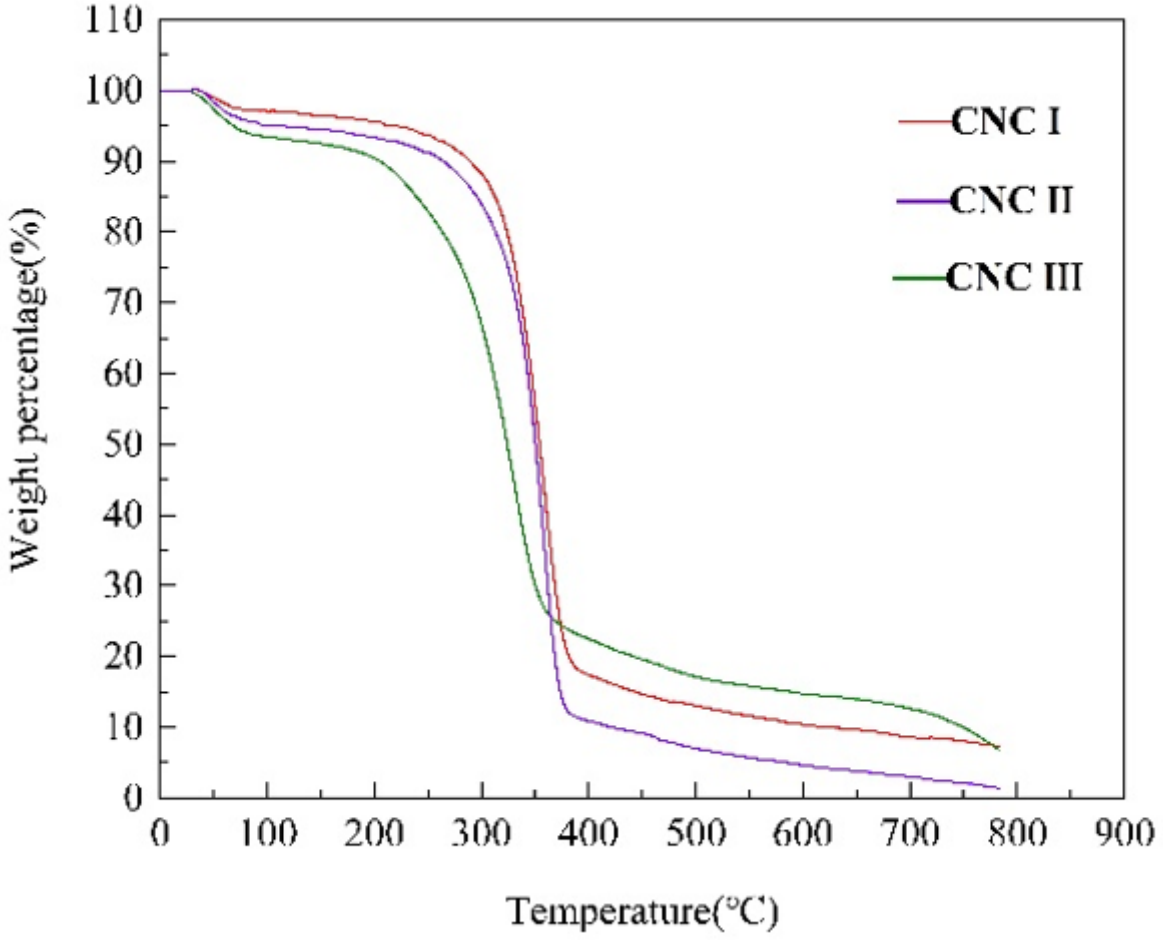

Figure 9

TGA pattens of samples